9700 *Inorg. Chem.* **2010**, *49*, 9700–9708
DOI: 10.1021/ic101521k

Inorganic Chemistry
Article

Magnetic Properties of Segregated Layers Containing $M^{II}_3(\mu_3-OH)_2$ (M = Co or Ni) Diamond Chains Bridged by *cis,cis,cis*-1,2,4,5-Cyclohexanetetracarboxylate

Mohamedally Kurmoo*

Laboratoire DECOMET, CNRS-UMR 7177, Université de Strasbourg, 4 rue Blaise Pascal, CS 90032, 67081 Strasbourg Cedex, France

Kazuya Otsubo† and Hiroshi Kitagawa†

Department of Chemistry, Graduate School of Science, Kyushu University, Hakozaki 6-10-1, Higashi-ku, Fukuoka 812-8581, Japan

Marc Henry

Laboratoire de Chimie Moléculaire de l'Etat Solide, CNRS-UMR 7140, Université de Strasbourg, 4 rue Blaise Pascal, CS 90032, 67081 Strasbourg Cedex, France

Masaaki Ohba‡

Department of Synthetic Chemistry and Biological Chemistry, Graduate School of Engineering, Kyoto University, Katsura, Nishikyo-ku, Kyoto 615-8510, Japan.

Seishi Takagi

Department of Physics and Electronics, Kyushu Institute of Technology, Kitakyushu, Fukuoka 804-8550, Japan. †*Present address: Division of Chemistry, Graduate School of Science, Kyoto University, Kitashirakawa-Oiwakecho, Sakyo-ku, Kyoto 606-8502, Japan, and Core Research for Evolutional Science and Technology (CREST), Japan Science and Technology Corporation (JST), Sanbancho 5, Chiyoda-ku, Tokyo 102-0075, Japan.* ‡*Present address: Department of Chemistry, Graduate School of Science, Kyushu University, Hakozaki 6-10-1, Higashi-ku, Fukuoka 812-8581, Japan.*

Received July 29, 2010

We report the hydrothermal synthesis, X-ray crystal structures, and thermal, optical, and magnetic properties of two isostructural layered coordination polymers, $[M^{II}_5(OH)_2(chtc)_2(H_2O)_{10}]\cdot 2H_2O$ where M = Co (**1Co**) or Ni (**2Ni**) and *chtc* = *cis,cis,cis*-1,2,4,5-cyclohexanetetracarboxylate. The structures consist of segregated layers where each layer is formed of $M_3(OH)_2$ diamond chains, involving edge- and corner-sharing octahedra, bridged by $M(chtc)_2$. In the space created by the chains and the bridges exists channels, which house the coordinated and noncoordinated water molecules, all hydrogen bonded to form a dodecamer, with a central cyclohexane chair shape ring. Interestingly, the water molecules of **2Ni** are more difficult to remove than those of **1Co**, but pyrolysis of the latter takes place at higher temperature. The magnetic properties are characterized by Néel transition to fully compensated antiferromagnets at 5.8 K (**1Co**) and 3.0 K (**2Ni**). The moments are easily reversed in an applied field of 150 Oe (**1Co**) and 300 Oe (**2Ni**) to a ferrimagnet with one uncompensated moment followed by a nonlinear increase to a saturation corresponding to a ferrimagnet with three uncompensated moments. Further, point charge calculations to estimate the weak bonding energies between the various types of interaction are reported.

Introduction

Layered materials have a special place in the chemistry of materials for their ability to take up molecules or exchange those in the galleries with other ones and also in physics for their large area display abilities and thin film technology.[1] As such, they have been applied in the field of chromatography and also in cleaning gases and solvents while they are used in displays and electrical circuitry and as optical filters.[1,2] In the natural world, these materials are classified as clays, and their

*To whom correspondence should be addressed. E-mail: kurmoo@unistra.fr.

 Published on Web 09/22/2010

structures are based principally on silicates.[3] Though many are inorganic and have been used for several applications, the most common and easily available organic is graphite. The latter finds its use due to its affinity for trapping organic molecules or gases and as solid-state lubricant due to the weak interlayer interaction.[4] The corresponding inorganic is zinc glycerolate that is largely used in the cosmetic and pharmaceutical industry due to the presence of zinc which repairs damaged skin.[5] Interestingly, most developments are directed toward inorganic layered materials due to the possibilities of their easily controlled syntheses and, importantly, their thermal and long-term stabilities. A large number of the designed inorganic materials are pillared by organic molecules which allowed for chemistry to be performed in the galleries as well as controlling the interlayer spacing; thus, their use is in catalysis.[3b,6] In contrast, stable segregated inorganic−organic hybrids held by electrostatic or hydrogen bonding or $\pi-\pi$ interactions are rather rare.

When the layers contain free electrons or magnetic moment carriers, a wide range of interesting electrical conductors and superconductors or magnets can be realized.[7,8] The designs and study of such materials form an integral part of the development for microelectronic, optical displays, and magnetic storage devices. From the point of view of magnetism, they provide exceptional characteristics in the field, given that many exhibit long-range magnetic ordering (LRO) while theoretically they should not.[9] These unexpected results have fascinated theoreticians and material designers for a long time. The most common explanation given for the LRO is the presence of weak magnetic exchange between the layers through bonds. When the chemical connection is absent between layers, dipolar interaction is usually suggested to be the reason.[10]

During our work over the past 15 years on magnetic coordination complexes with both inorganic and organic ligands, we have encountered several layered structures that behave as magnets and, in some cases, with some very peculiar temperature and magnetic field dependences not encountered before.[11] The ground state can be ferromagnetic, ferrimagnetic, antiferromagnetic with metamagnetic transformation, or canted antiferromagnetic. The critical temperatures can reach 60 K, and the coercive field exceptionally exceeds 50 kOe at 2 K in some metamagnetic cases. Among them, the pillared layer compounds are the most frequent; these include $Co_5(OH)_6(ZO_4)_2(H_2O)_4$, Z = S or Se,[12] $Co_5(OH)_8chdc\cdot 4H_2O$, *chdc* = *trans*-1,4-cyclohexanedicarboxylate,[13] $Co_2(OH)_2bdc$, *bdc* = 1,4-benzenedicarboxylate (terephthalate),[14] $Co_2(btec)$, *btec* = 1,2,4,5-benzenetetracarboxylate (pyromellitate),[15] and $Co_8(OH)_6(SO_4)_2(L)\cdot nH_2O$, *L* = ethylenediamine or dabco.[16] To understand the observed magnetic properties of the above compounds, we extended our study for known segregated layer structures which include $Co(OH)_2$, $Co_2(OH)_3NO_3$,[17] and Co-glycerolate.[18] The aim of the present study was originally to replace pyromellitate with 1,2,4,5-cyclohexanetetracarboxylate, as we have already done for terephthalate to 1,4-cyclohexanedicarboxylate and trimesate to 1,3,5-cyclohexanetricarboxylate.[19] The present outcome was quite surprising, and here, we describe the structures of the two complexes, their thermal and optical properties, and extensive magnetic measurements to elucidate their unique properties that are characterized by metamagnetism below Néel

(1) (a) Leith, R. M. A. *Preparation and crystal growth of materials with layered structure*; D. Reidel Publisher: Dordrecht, 1977. (b) Jacobson, A. J. In *Solid state chemistry: Compounds*; Oxford University Press: Oxford, 1992. (c) Pinnavaia, T. J. *Science* **1983**, *220*, 365. (d) Schoellhorn, R. *Inclusion Compd.* **1984**, *1*, 249. (e) Clearfield, A. *Curr. Opin. Solid State Mater. Sci.* **1996**, *1*, 268. (f) Clearfield, A. *Chem. Rev.* **1988**, *88*, 125. (g) Clearfield, A. *Prog. Inorg. Chem.* **1998**, *47*, 371. (h) Cao, G.; Hong, H.; Mallouk, T. E. *Acc. Chem. Res.* **1992**, *25*, 420. (i) Gavin, J. A. *Acc. Chem. Res.* **1998**, *31*, 209. (j) O'Hare, D. In *Inorganic materials*; Bruce, D. W., O'Hare, D., Eds.; Wiley: London, 1993.

(2) (a) Mitchell, I. V., Ed. *Pillared layered structure: Current trends and applications*; Elsevier: London, 1990. (b) Heinrich, B.; Bland, J. A. C., Eds. *Ultrathin magnetic structures*; Springer-Verlag: Berlin, 1994. (c) Makiura, R.; Motoyama, S.; Umemura, Y.; Yamanaka, H.; Sakata, O.; Kitagawa, H. *Nat. Mater.* **2010**, *9*, 565.

(3) (a) Bailey, S. W. In *Crystal Structures of Clay Minerals and their X-ray Identification*; Brindley, G. W.; Brown, G., Eds. Monograph 5; Mineralogical Society: London, 1980; p 1. (b) Corma, A. *Chem. Rev.* **1997**, *97*, 2373. (c) Kloprogge, J. T. *J. Porous Mater.* **1998**, *5*, 5.

(4) (a) Pierson, H. O. *Handbook of Carbon, Graphite, Diamonds and Fullerenes: Processing, Properties and Applications* (*Materials Science and Process Technology*); Noyes Publication, 1993. (b) Feneberger, K. *Ind. Lubr. Tribol.* **1993**, *25*, 176.

(5) (a) Radoslovich, E. W.; Raupach, M.; Slade, P. G.; Taylor, R. M. *Aust. J. Chem.* **1970**, *23*, 1963. (b) Taylor, R. M.; Brock, A. J. U.S. Patent 4 87 378, 1989. (c) Whitehouse, M. W.; Rainsford, K. D.; Taylor, R. M.; Vernonroberts, B. *Agents Actions* **1990**, *31*, 47.

(6) Rives, V., Ed. *Layered double hydroxide, present and future*; Nova Science Publishers, 2001. (b) Clearfield, A. *Solvent Extr. Ion Exch.* **2000**, *18*, 655.

(7) (a) Ishiguro, T.; Yamaji, K.; Saito, G. *Organic Superconductors*, 2nd ed.; Springer Verlag: Telos, 1998. (b) Kurmoo, M.; Graham, A. W.; Day, P.; Coles, S. J.; Hursthouse, M. B.; Caulfield, J. L.; Singleton, J.; Pratt, F. L.; Hayes, W.; Ducasse, L.; Guionneau, P. *J. Am. Chem. Soc.* **1995**, *117*, 12209. (c) Coronado, E.; Galan-Mascaros, J. R.; Gomez-Garcia, C. J.; Laukhin, V. *Nature* **2000**, *408*, 447. (d) Mourachkine, A. *Room-Temperature Superconductivity*; Cambridge International Science Publishing: Cambridge, UK, 2004.

(8) (a) Bellitto, C.; Day, P. *J. Mater. Chem.* **1992**, *2*, 265. (b) Tamaki, H.; Zhong, Z. J.; Matsumoto, N.; Kida, S.; Koikawa, M.; Achiwa, N.; Hashimoto, Y.; Okawa, H. *J. Am. Chem. Soc.* **1992**, *114*, 6974. (c) Decurtins, S.; Schmalle, H. W.; Schneuwly, P.; Ensling, J.; Gütlich, P. *J. Am. Chem. Soc.* **1994**, *116*, 9521. (d) Mathoniere, C.; Carling, S. G.; Yusheng, D.; Day, P. *J. Chem. Soc., Chem. Commun.* **1994**, 1551. (e) Nuttall, C.; Day, P. *Chem. Mater.* **1998**, *10*, 3050. (f) De Jongh, L. J. A.; Batterman, C.; Bose, F. R.; Miedema, A. R. *J. Appl. Phys.* **1969**, *40*, 1363. (g) Miedema, A. R.; van Kempen, H.; Huiskamp, W. J. *Physica* **1963**, *29*, 1266. (h) Clement, R.; Lacroix, P.; Evans, J. S. O.; O'Hare, D. *Adv. Mater.* **1994**, *6*, 794. (i) De Jongh, L. J.; Miedema, A. R. *Adv. Phys.* **1974**, 23. (j) Day, P., Underhill, A. E., Eds. *Metal-Org. Org. Mol. Magnets, Philos. Trans. R. Soc. London, Ser. A*, **1999**, *357*, 1.

(9) De Jongh, L. J., Ed. *Magnetic Properties of Layered Transition Metal Compounds*; Kluwer Academic Publishers: Dordrecht and Boston, MA, 1990.

(10) De'Bell, K.; MacIsaac, A. B.; Whitehead, J. P. *Rev. Mod. Phys.* **2000**, *72*, 225.

(11) Kurmoo, M. *Chem. Soc. Rev.* **2009**, *38*, 1353.

(12) (a) Ben Salah, M.; Vilminot, S.; Andre, G.; Richard-Plouet, M.; Mhiri, T.; Takagi, S.; Kurmoo, M. *J. Am. Chem. Soc.* **2006**, *128*, 7972. (b) Wassim, M.; Vilminot, S.; André, G.; Kurmoo, M. *Inorg. Chem.* **2010**, *49*, 3019.

(13) Kurmoo, M.; Kumagai, H.; Hughes, S. M.; Kepert, C. J. *Inorg. Chem.* **2003**, *42*, 6709.

(14) (a) Kurmoo, M.; Kumagai, H.; Green, M. A.; Lovett, B. W.; Blundell, S. J.; Ardavan, A.; Singleton, J. *J. Solid State Chem.* **2001**, *159*, 343. (b) Kurmoo, M.; Kumagai, H. *Mol. Cryst. Liq. Cryst.* **2002**, *376*, 555. (c) Lovett, B. W.; Blundell, S. J.; Kumagai, H.; Kurmoo, M. *Synth. Met.* **2001**, *121*, 1814.

(15) Kumagai, H.; Kepert, C. J.; Kurmoo., M. *Inorg. Chem.* **2002**, *41*, 3410.

(16) (a) Rujiwatra, A.; Kepert, C. J.; Rosseinsky, M. J. *Chem. Commun.* **1999**, 2307. (b) Rujiwatra, A.; Kepert, C. J.; Claridge, J. B.; Rosseinsky, M. J.; Kumagai, H.; Kurmoo, M. *J. Am. Chem. Soc.* **2001**, *123*, 10584.

(17) (a) Kurmoo, M. *Philos. Trans. R. Soc., London A* **1999**, *357*, 3041. (b) Kurmoo, M. *Mol. Cryst. Liq. Cryst.* **2000**, *341*, 1199. (c) Kurmoo, M. *Chem. Mater.* **1999**, *11*, 3370. (d) Kurmoo, M. *Mol. Cryst. Liq. Cryst.* **2000**, *342*, 167. (e) Jestädt, T.; Kurmoo, M.; Blundell, S. J.; Lovett, B. W.; Pratt, F. L.; Hayes, W. *Synth. Met.* **1999**, *103*, 2325. (f) Kurmoo, M. *J. Mater. Chem.* **1999**, *9*, 2595.

(18) Pratt, F. L.; Baker, P. J.; Lancaster, T.; Green, M. A.; Kurmoo, M. *Phys. Rev. Lett.* **2007**, *99*, 017202.

(19) Kumagai, H.; Akita-Tanaka, M.; Inoue, K.; Kurmoo, M. *J. Mater. Chem.* **2001**, *11*, 2146.

transition of 5.8 K (**1Co**) and 3.0 K (**2Ni**). The structure of the cobalt compound and a preliminary study of the magnetism have recently been reported.[20]

Experimental Section

Synthesis of $[M_5(OH)_2(cis,cis,cis\text{-}1,2,4,5\text{-}chtc)_2(H_2O)_{10}]\cdot 2H_2O$. All the starting materials employed were commercially available and used as received without further purification. The acid is available as a mixture of the *cis*- and *trans*-isomer. A general procedure was employed where a solution of $MCl_2\cdot 6H_2O$ (25 mg) was mixed to a neutralized solution of 50 mg of the *cis*- and *trans*-1,2,4,5-cyclohexanetetracarboxylic acid (1,2,4,5-*chtc*H_4) followed by an aqueous NaOH solution (0.4 mM/cm^3). The slurry was placed in a 12 mL autoclave and heated at 120 °C for 12 h. A higher temperature of 170 °C also works well for the nickel compound but less well for the cobalt one. The reactions yield purple platelike crystals of **1Co** or a light green microcrystalline powder of **2Ni**, both in single phase. Phase purity of the bulk materials was confirmed by comparison of their powder diffraction (XRPD) patterns with those calculated from single crystal X-ray diffraction study. Elemental analyses calcd. (%) for $C_{20}H_{42}O_{30}Co_5$ (**1Co**): C, 22.72; H, 4.00. Found: C, 22.65; H, 4.03. calcd. (%) for $C_{20}H_{42}O_{30}Ni_5$ (**2Ni**): C, 22.75; H, 4.01. Found: C, 22.63; H, 4.05.

Physical Measurements. The C, H, and N microanalyses were carried out at the Elemental Analysis Service Center of Kyushu University, Fukuoka, Japan. Thermal analyses (DT and thermogravimetric analysis, TGA) under nitrogen were measured on a Bruker TG-DTA 2020SA for samples heated at a rate of 1 °C/min. The Fourier transform infrared spectroscopy (FTIR) spectra were recorded from KBr pellets in the range of 400−6000 cm^{-1} on a Thermo Fisher NEXUS 670 FTIR.

Direct current (dc) magnetic susceptibility measurements were performed on polycrystalline samples using four different Quantum Design MPMS SQUID magnetometers equipped with 50 or 70 kOe magnets. Magnetization measurements were performed in the 2−300 K temperature range and the applied field of ±70 kOe. Ac magnetic susceptibility measurements were obtained using 2 Oe alternating current (ac) field at a frequency 17 Hz and zero applied dc magnetic field. Data were corrected for diamagnetism estimated from Pascal's constants.

X-ray Crystallography. A single crystal of **1Co** was selected and placed on a glass fiber for data collection at 173 K on a Bruker APEX CCD diffractometer equipped with Mo Kα radiation. The intensities were corrected for absorption semiempirically. The structure was solved by direct methods and refined using SHELX. All atoms except hydrogen were refined with anisotropic thermal factors. A summary of the data collection and crystal structure analysis is given in Table 1. Several of the hydrogen atoms were found in the difference Fourier maps, and the rest were placed theoretically and refined using the riding model. The cif file has been deposited at the Cambridge Crystallographic Data Centre, 12 Union Road, Cambridge CB21EZ, U.K.; Fax: (+44) 1223−336−033. These data can be obtained free of charge via www.ccdc.cam.ac.uk/conts/retrieving.html or by mailing at deposit@ccdc.cam.ac.uk.

XRPD were recorded for samples of **1Co** and **2Ni** from several individual batches at 295 K using a large imaging plate Debye−Scherrer camera installed on the BL02B2 beamline (λ = 0.69153 Å) at SPring-8, Japan. The powders were held in 0.5 mm diameter capillary tubes. Analyses of the data were performed using Reitveld refinement within the TOPAS program.[21] As the powder pattern of **2Ni** was the same as that of **1Co**, the structure was finally solved starting from the atomic coordinate found in the single crystal structure determination of **1Co**.

Table 1. Summary of the Crystallographic Data

compound	1Co	2Ni
formula	$C_{20}H_{42}Co_5O_{30}$	$C_{20}H_{42}Ni_5O_{30}$
formula weight	1057.19	1056.00
state	single crystal	powder
T, K	173	298
λ, Å	0.71073	0.69153
crystal system	monoclinic	monoclinic
space group	$P\,2_1/c$	$P\,2_1/c$
a, Å	10.2251(11)	10.17350(23)
b, Å	6.5516(6)	6.50033(16)
c, Å	24.394(3)	24.44335(50)
β, °	92.021(2)	91.8446(17)
V, Å^3	1633.1(3)	1615.627(63)
Z	2	2
D_c, g/cm^3	2.150	2.170
μ (Mo Kα), mm^{-1}	2.606	
crystal size, mm^3	0.08 × 0.08 × 0.05	
T_{min} and T_{max}	0.8186, 0.8807	
θ_{min} and θ_{max}, deg	3.34 to 29.53°	
total no. of reflections	14346	
no. of unique reflections (R_{int})	4509	
no. of observed [$I \geq 2\sigma(I)$]	4509	
no. of restraints/parameters	9/282	
R1/wR2 [$I \geq 2\sigma(I)$]	0.0337, 0.0501	R_{Bragg} = 0.593 R_{exp} = 1.40 R_{wp} = 1.80 R_p = 1.19
R1/wR2 (all data)	0.0685, 0.0541	
GOF	1.043	1.28
$\Delta\rho$ e/Å^3	−0.459, 0.543	

Table 2. M−O Bond Lengths (Å) for **1Co** and **2Ni**

	1Co	2Ni		1Co	2Ni
M(1)−O(1)	2.0267	1.977	M(1)−O(7)	2.0438	1.938
M(1)−O(9)	2.0979	2.054	M(1)−O(9)	2.1145	2.072
M(1)−O(11)	2.1610	2.184	M(1)−O(10)	2.2421	2.118
M(2)−O(3)	2.0612	2.072	M(2)−O(5)	2.0916	1.984
M(2)−O(13)	2.0954	2.116	M(2)−O(12)	2.1078	2.114
M(2)−O(14)	2.116	2.136	M(2)−O(6)	2.1513	2.228
M(3)−O(9)	2.0487	2.116	M(3)−O(8)	2.1215	2.054
M(3)−O(2)	2.1587	2.174			

Results and Discussion

Synthesis. For the syntheses of the compounds, we have varied the time and temperature of the reactions as well as the concentration of the base. While there seems to be little effect of increasing the base concentration in the case of **2Ni**, for **1Co**, other unidentified phases appear at high concentration in addition to the formation of oxides. The latter is present in higher quantity at higher temperatures. XRPD indicate that at 120 °C the only identifiable phases are those of the two compounds. Thus, all the samples used for the characterization were prepared at 120 °C. In the case of **2Ni**, another low quality crystalline phase {$[Ni(H_2O)_6](H_2chtc)\cdot H_2O$, *Pbca*, a = 11.8101(17), b = 12.2759(19), c = 23.431(3) Å, V = 3397.0(9) Å^3, Z = 8, R1 = 0.122, Rw = 0.3227, GOF = 1.056} is obtained from the mother liquor at near dryness.

Crystal Structures. The two compounds are isostructural and differ only in dimensions due to the different ionic radii of the metal, where the bond distances and lattice parameters are smaller for **2Ni**. Therefore, we will only describe the structure of the cobalt compound as the

(20) Wang, R.; Zhang, J.; Li, L. *Inorg. Chem.* **2009**, *48*, 7194.
(21) Bruker AXS, *TOPAS V3*: General profile and structure analysis software for powder diffraction data; Bruker AXS: Karlsruhe, Germany, 2005.

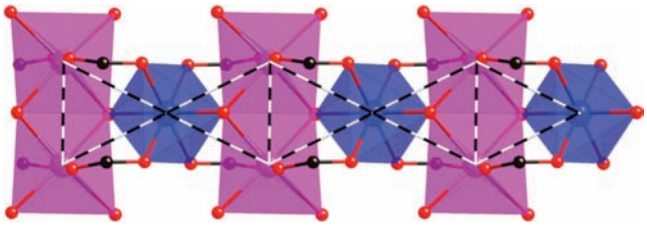

Figure 1. $Co_3(OH)_2$ chain with the magnetic exchange pathways highlighted (dotted line).

structure was obtained from single crystal diffraction, and for the related details of the nickel compound, see Tables 1 and 2 and the CCDC deposited data. We will also keep the description short as the structure has been reported but highlight the details relevant for the understanding of the magnetic properties.[20] The key feature of the structures is the presence of segregated layers containing the inorganic M−O−M chains that are bridged by the organic acid. Importantly, within the layers the inorganic building block, that is $M_3(\mu_3{-}OH)_2$, chains (Figure 1) are parallel and the magnetic topology is that of a diamond chain. This particular chain topology is found in several metal−organic hybrids of divalent transition metals, Mn, Co, and Ni, where the organic is fumarate,[22] 1,4-cyclohexanedicarboxylate,[23] and others.[11] A slight variant is known for minerals, $A_2M_3(OH)_2(SO_4)_3(H_2O)$, where A = Na or K and M = Mn, Fe, Co, and Ni.[24]

The asymmetric unit contains three crystallographically independent Co(II) atoms where Co1 lies on special position and Co2 and Co3 lie on general positions, a *chtc*, a μ_3−OH, and five coordinated water molecules and one lattice water molecule (see Figure S1, Supporting Information). The diamond chains consist of two symmetry equivalent Co1 atoms (purple in Figure 2) and one Co3 (blue in Figure 2) where their coordination numbers are six. The Co1 octahedra are edge-shared through the two hydroxide, and they are corner-shared by the Co3 through the same hydroxide. Thus, the hydroxide has μ_3 coordination. Co1 has two carboxylate oxygen atoms in *trans*-positions and two water molecules in *cis*-positions. Co3 has four carboxylate oxygen atoms to complete it's coordination sphere. All three octahedra are slightly distorted with bond distances ranging from 2.027 to 2.16 Å (Table 2) and angles of 62 to 97°, where the distances and angles are normal. The lowest angle is that with the chelating carboxylate. The connection between the chains is mediated by the *cis,cis,cis*-1,2,4,5-*chtc* which adopts the *a,a,e,e* boat conformation, as that in the structure of the pure acid.[25] Thus, the axial carboxylate groups are involved in the coordination to the $Co_3(\mu_3{-}OH)_2$ chains and the equatorial ones bridged the chains via the Co2 atom (green in Figures 2 and S1, Supporting Information). While the two axial carboxylate groups bridge the Co1 and Co3 within the chain, one of the equatorial ones chelate Co2 and the other is monodentate to Co2.

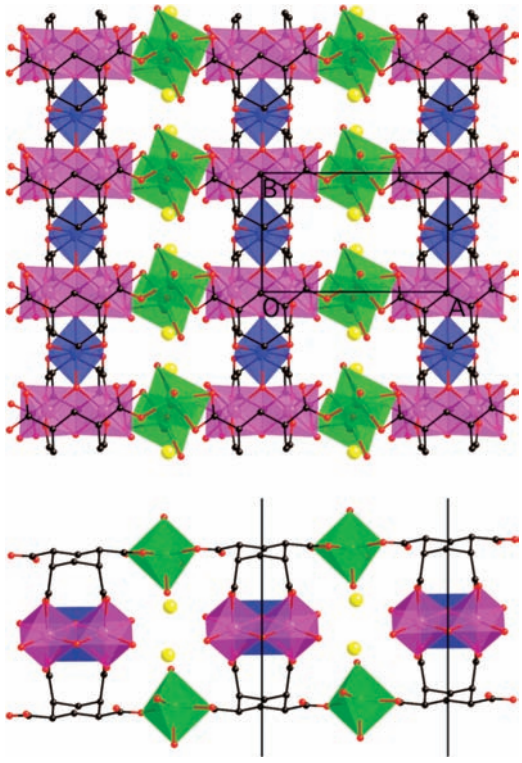

Figure 2. (a) Top view of one layer along the *c*-axis, (b) side view along the *b*-axis showing the $Co_3(OH)_2$ chains (purple, Co1, and blue, Co3) bridged by the $Co(H_2O)_3$−carboxylate (green, Co2) and the lattice water molecules (yellow).

Because of the strained chelate angle imposed by the carboxylate on Co2 and the presence of three meridial water molecules, the octahedral is the most distorted. The resulting layer, thus, consists of central and parallel $Co_3(\mu_3{-}OH)_2$ chains connected via the Co−(*chtc*)$_2$ bridges. The square shaped channels that are created by this particular arrangement results in a surface of water molecules. The lattice water molecules occupy these channels forming dodecamers $(H_2O)_{12}$ with O···O distances as short as 2.57 Å (Figure 3) with the coordinated water molecules. This provides a hydrogen-bonded pathway between the $Co_3(\mu_3{-}OH)_2$ chains. The Co···Co distances (Table 3) are the shortest (3.1 Å) for the edge-shared dimer followed by the corner sharing (3.6 Å) and then between the chain and monomer Co2 (5.4−6.6 Å). The shortest Co···Co distance between different layers is 5.0 Å. The Reitveld refinement of the structure of the **2Ni** is shown Figure 4 for a structure analogous to that of **1Co**. The relevant distances and angles are given in Tables 2 and 3.

Thermal Properties. The DT and TG analyses under nitrogen are shown in Figure 5. The first weight loss is associated with the departure of six water molecules, and the process is endothermic. There is a difference of 50 °C between that of **1Co** and **2Ni** which is commonly observed. This difference is interpreted as being due to the stronger Ni−O than the Co−O bond which may be a consequence of the electronic configuration and ionic radii of the metal. The second process is very gradual and so has lower heat associated to it. The difference in the second loss between the two compounds is also as marked as the previous one. The amount of water loss for the second anomaly is also six. The third weight loss is the

(22) Konar, S; Mukherjee, P. S.; Zangrando, E.; Lloret, F.; Chaudhuri, N. R. *Angew. Chem., Int. Ed.* **2002**, *41*, 1561.
(23) Kurmoo, M.; Kumagai, H.; Akita-Tanaka, M.; Inoue, K.; Takagi, S. *Inorg. Chem.* **2006**, *45*, 1627.
(24) Vilminot, S.; Baker, P. J.; Blundell, S. J.; Sugano, T.; André, G.; Kurmoo, M. *Chem. Mater.* **2010**, *22*, 4090.
(25) Uchida, A.; Hasegawa, M.; Manami, H. *Acta Crystallogr.* **2003**, *C59*, o435.

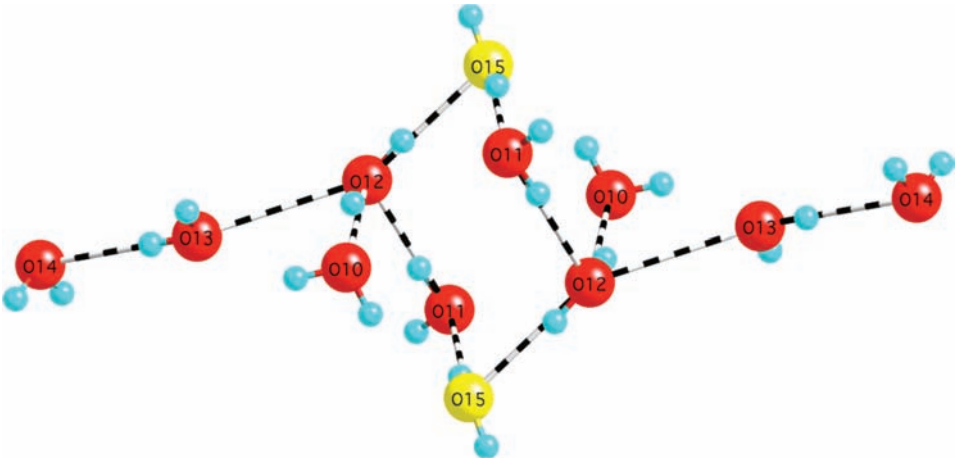

Figure 3. Hydrogen-bonded network in the water molecule cluster.

Table 3. M−M Distances (Å) and M−O−M Angles (°)

	1Co	2Ni
M(1)−M(1)	3.116	3.078
M(1)−M(3)	3.623, 3.631	3.591, 3.601
M(1)−M(2)	5.483, 5.594	5.472, 5.575
M(2)−M(2) (intralayer)	6.500, 8.496	6.552, 8.467
M(2)−M(2) (interlayer)	5.043	5.063
M(1)−O(9)−M(1)	95.41	96.31
M(1)−O(9)−M(3)	121.44	118.03
M(1)−O(9)−M(3)	121.78	119.08

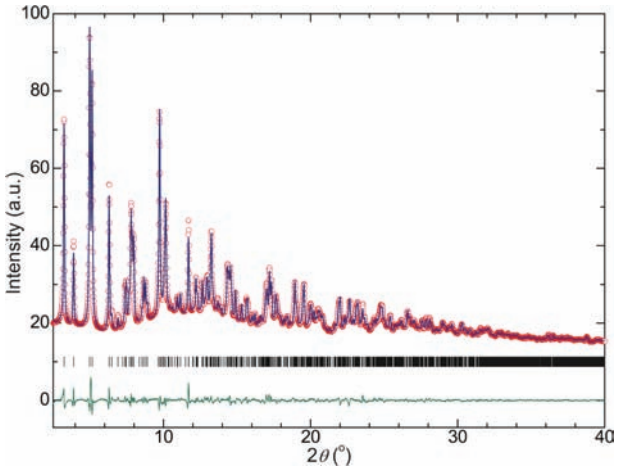

Figure 4. Experimental X-ray powder diffraction (red circles) and Rietveld refined (blue line) and difference patterns (green line) for **2Ni** (λ = 0.69153 Å). The ticks are the position of the Bragg reflections, and the bottom trace is the residual.

pyrolysis of the compounds with the departure of the organic moiety leaving the divalent metal oxide as residues. Interestingly, the pyrolysis process for **2Ni** takes place at a lower temperature than that for **1Co**, which may be an indication that the Ni−O(carboxylate) bond is weaker than that of Co−O(carboxylate).

Infrared Spectroscopy. The infrared spectra of the two compounds (Figure 6) show well-defined peaks that can be assigned using group frequencies of the various fragments, hydroxide, water, carboxylate, and the cyclohexane.[26] We

(26) (a) Deacon, G. B.; Phillips, R. J. *Coord. Chem. Rev.* **1980**, *33*, 227. (b) Nakamoto, K. *Infrared and Raman Spectra of Inorganic and Coordination Compounds*; 5th ed.; John Wiley and Sons: New York, 1997.

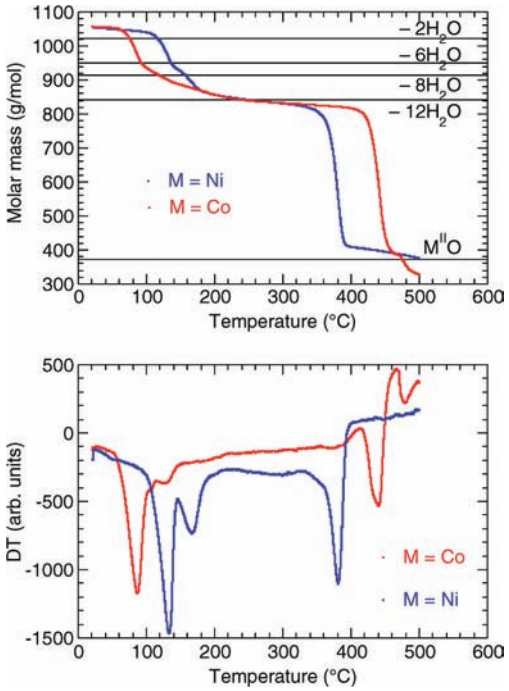

Figure 5. TGA (top) and DT (bottom) for **1Co** and **2Ni** measured under nitrogen.

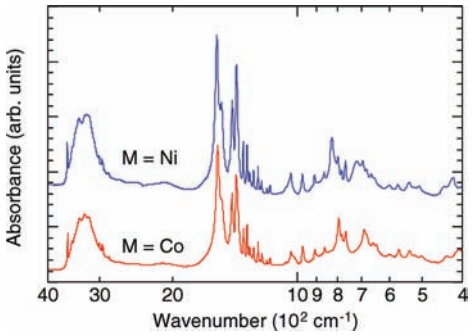

Figure 6. Infrared spectra of **1Co** and **2Ni**.

note that there are two sets of bands; one where the bands are at the same frequencies for the two compounds and the second set where they do vary. The OH mode is assigned

to the sharp band at the highest energy 3586 cm^{-1} (**1Co**) and 3590 cm^{-1} (**2Ni**). The water stretching modes are heavily overlapped and broad in the region 3180−3368 cm^{-1}, and one can identify three bands that may be from the three types of water molecules (lattice and coordinated to two crystallographic different metals). The CH modes are weak and clustered around 2850−3230 cm^{-1}. The carboxylate modes are associated to the strongest bands in the spectra at 1556 and 1524 cm^{-1} (**1Co**) and 1564 and 1525 cm^{-1} (**2Ni**) for the antisymmetric vibrations and at 1438 and 1404 cm^{-1} (**1Co**) and 1436 and 1402 cm^{-1} (**2Ni**) for the symmetric vibrations. The fine structures in these bands are due to the different coordination modes of the carboxylate groups. Two other metal-sensitive bands are observed at 790 and 686 cm^{-1} (**1Co**) and 826 and 719 cm^{-1} (**2Ni**). These are assigned to the OCO bending modes. The metal−oxygen core vibrations are weak and observed at 436 and 409 cm^{-1} (**1Co**) and 442 and 422 cm^{-1} (**2Ni**).

Estimation of the H-Bond Energies for the $\{(H_2O)_{12}\}$ Cluster[27]. The presence of this water cluster provides the opportunity to estimate the energies involved in the hydrogen bonding that stabilizes such geometry. Before computations, all C−H and O−H bond lengths obtained from the X-ray analyses have been scaled at their standard value (1.08 and 0.97 Å, respectively). The lattice energy of this structure was found to be $EB_{net} = -13\,540.0$ $kJ.mol^{-1}$, leading to an average global ionicity of 18.4%. Considering only the $\{H_2O\}_{12}$ water cluster, it may be described as a $\{H_2O\}_8$ water cube with two missing edges augmented by two pairs of water dimers located in *trans* positions (Figure 7a).

The $\{H_2O\}_{12}$ relaxed water cluster (Figure 7b) was obtained by minimizing in the vacuum the electrostatic energy of a system of 24 H atoms moving around a fixed array of 12 O atoms and submitted to 24 bond lengths (d_{O-H} = 97 pm) and 12 bond angles constraints (θ_{H-O-H} = 104.5°). At convergence on this 36-D energy surface, the final topology was found to be very similar to that observed in the solid state. This clearly demonstrates that the dimer-buttressed open-cube topology arises from water/water interactions alone and is not imposed by the coordination of some water molecules to the Co atoms. The encapsulating framework then plays the important role of a molecular container ruling the number of water molecules and the relative spatial disposition of the O atoms but has a rather weak influence on the H-bond pattern that is ruled by hydrogen-mediated many-body effects. This is fully confirmed by the observation that, as in the solid-sate, monomers and dimers cooperate with undecamers and decamers, whereas the anticooperation between trimers and nonamers appears to be significantly reduced. The quite strong cooperation between monomers within the 32 constituting trimers is again observed, but now monomers are found to cooperate also within the 14 constituting dimers. As expected, relaxation in the vacuum has a neat stabilizing effect (more negative H-bond energy) and reinforces the cooperation between water molecules.

(27) (a) Henry, M. *ChemPhysChem* **2002**, *3*, 607. (b) Henry, M. *J. Cluster Sci.* **2002**, *13*, 437.

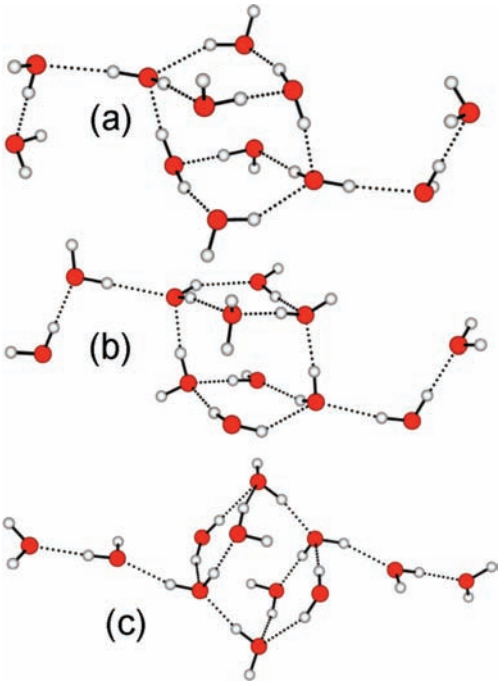

Figure 7. Three topologies evidenced in the $[Co_5\ (\mu_3-OH)_2(chtc)_2(H_2O)_{10}]\cdot 2H_2O$ framework. (a) Observed encapsulated open cube with long O···O contacts (304 pm) between water dimers and the open cube: <O···O> = 287(14) pm, <O−H···O> = 10(8)°, EB_{12} = −2378.5, $E_{HB}(14)$ = −21.1, ΔE_{12} (1,11) = −11.2, ΔE_{12} (2,10) = −8.0, ΔE_{12} (3,9) = +31.9 (T = 32), ΔE_{12} (1,1) = +2.6, and ΔE_{12} (1,1,1) = −47.0. (b) Same dodecameric cluster after relaxation of H atoms in the vacuum in skewed positions: <O···O> = 287(14) pm, <O−H···O> = 8(8)°, EB_{12} = −2400.0, $E_{HB}(14)$ = −25.0, ΔE_{12} (1,11) = −11.2, ΔE_{12} (2,10) = −24.3, ΔE_{12} (3,9) = +15.3 (T = 32), ΔE_{12} (1,1) = −6.2, and ΔE_{12} (1,1,1) = −43.7. (c) Same dodecameric cluster after relaxation of H atoms in the vacuum in linear positions: <O···O> = 284(11) pm, <O−H···O> = 10(6)°, EB_{12} = −2420.6, $E_{HB}(14)$ = −26.4, ΔE_{12} (1,11) = −14.9, ΔE_{12} (2,10) = +3.1, ΔE_{12} (3,9) = +28.4 (T = 32), ΔE_{12} (1,1) = −26.1, and ΔE_{12} (1,1,1) = −53.9. All energy units are in kJ/mol.

It is worth noticing that in the above clusters the O···O distances between the two water dimers H bonded to the water cube (Figure 7a) are rather long (304 pm). In fact, ignoring H atoms, it is possible to isolate from the crystal structure another water dodecamer characterized by the same topology but with a significantly shorter O···O distance (284 pm) and much wider O···O···O angle (153°). As before, the electrostatic energy of a system of 24 H atoms moving around this new fixed array of 12 O atoms and submitted to 24 bond lengths (d_{O-H} = 97 pm) and 12 bond angles constraints (θ_{H-O-H} = 104.5°) has been minimized in the vacuum. At convergence on this new 36 D energy surface, a more stable water dodecamer was obtained (Figure 7c). However, in contrast with the cluster shown in Figure 7b, there is now a neat anticooperation of dimers with decamers and more anticooperation of trimers with nonamers. Other many-body indexes point to quite strong cooperation of individual water monomers with undecamers or with other monomers. Consequently, with two possible alternatives existing in the network leading to the appearance of a H-bonded water dodecamer having the same topology of a dimer-buttressed open cube, the presence of the encapsulating framework seems to favor the least stabilized isomer where dimers fully cooperate. This selection of the longest O···O contacts (304 pm) in preference to

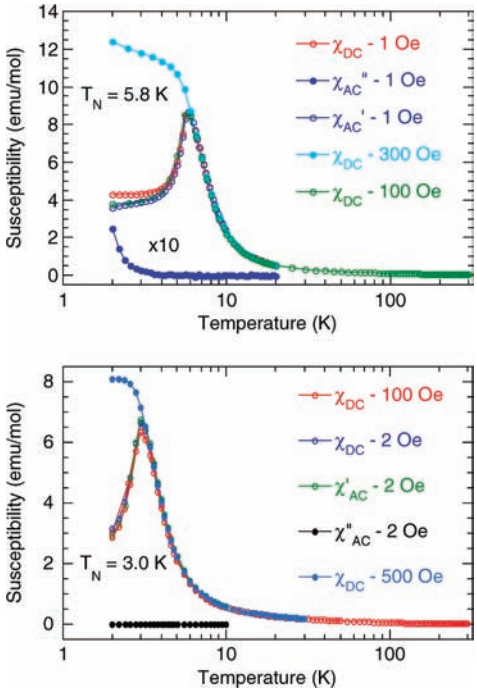

Figure 8. Ac and dc magnetic susceptibilities for **1Co** (top) and **2Ni** (bottom) measured under different applied magnetic fields.

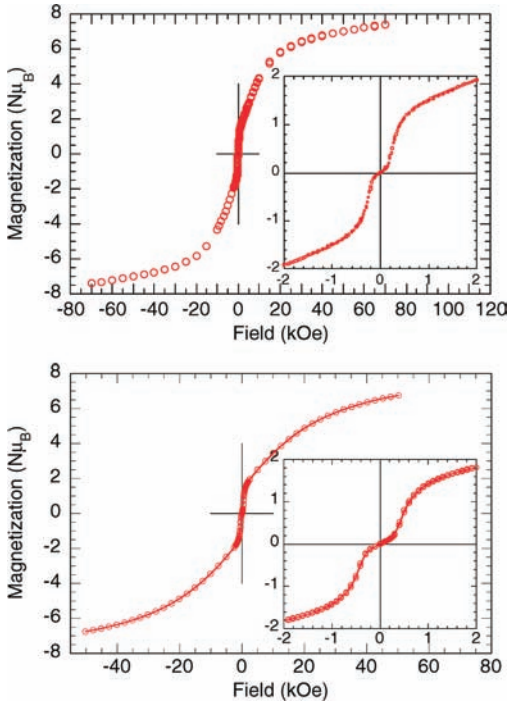

Figure 9. Isothermal magnetization at 2 K for **1Co** (top) and **2Ni** (bottom).

the shortest ones (284 pm) during the creation of the $\{H_2O\}_{12}$ dodecamer is quite counterintuitive and demonstrates that nonadditive many-body effects should not be overlooked when discussing water clustering in the solid state.

Magnetic Properties. The magnetic properties of the two compounds have been studied employing different experimental protocols and using both ac and dc mode. The dc susceptibilities were first measured in an applied field of 100 Oe on cooling from 300 to 2 K. The results are shown in Figures 8 and 9. Curie−Weiss fits of the data in the high temperature region give the following: **1Co**, 100−300 K, $C = 15.88(5)$ emu K/mol, and $\Theta = -43(1)$ K; and **2Ni**, 50−300 K, $C = 5.87(2)$ emu K/mol, and $\Theta = -6.1(7)$ K. The Curie constants are well within the experimentally observed ranges of these ions.[28] The negative values of the Weiss constants suggest antiferromagnetic interaction dominates the high temperature region. However, at low temperatures, a clear drop in susceptibility is observed in each case. The value at the lowest temperature (2 K) is approximately half that at the peak. These anomalies occur at 5.8 K for **1Co** and 3.0 K for **2Ni**. Measurements using lower applied fields of 1 Oe (**1Co**) and 2 Oe (**2Ni**) reproduce the same curves, except that for the former there is a slight difference below 4 K. In a higher applied field of 300 Oe (**1Co**) and 500 Oe (**2Ni**), the anomalies are suppressed and the susceptibilities tend to a saturation. This behavior is consistent with metamagnetism, thus confirming the anomalies to the Néel transition. The ac susceptibilities were measured using an applied ac field of 2 Oe oscillating at 17 Hz and zero dc field. The real component of the ac susceptibilities reproduces the dc susceptibilities in 100 Oe in both cases. However, for the **2Ni**, the imaginary component remains zero at all temperatures and that for the **1Co** increases from zero below 4 K.

The behavior of the isothermal magnetization at 2 K of the two compounds has some similarities (Figure 9) and shows first a sigmoidal shape with a change of slope at 150 Oe (**1Co**) and 300 Oe (**2Ni**) followed by a plateau of ca. 2 μ_B in both cases before gradually increasing nonlinearly to saturation values of 7.4 μ_B (**1Co** at 70 kOe) and 6.7 μ_B (**2Ni** at 50 kOe). Also noticeable is a slight hysteresis above the metamagnetic critcal field in each case.

These magnetic properties appear to be unusual at first sight, but some of the observations are interpretable while others can only be speculated.[29] We can be sure that the two compounds are antiferromagnets below the respective Néel temperature and that some of the moments can be reversed with a field superior to the metamagnetic critical one.[30] However, the nonlinear second rise in magnetization above 5 kOe is unusual and deserves some comments.

The isothermal magnetization becomes more straightforward using previous results related to compounds having such chains of cobalt and nickel where it is well-established that each chain behaves in a ferrimagnetic fashion with the moments of the edge-sharing pair (M1) ferromagnetically coupled and the corner-sharing one (M3) antiferromagnetically coupled to them.[11,22,23] In the present case, the complete compensation of the resulting moments can be interpreted in two ways (Figure 10). One is where the corresponding moments of adjacent

(28) (a) Herpin, A. *Theorie du Magnetisme*; Presses Universitaire de France: Paris, 1968. (b) Griffiths, J. S. *The theory of transition-metal ions*; Cambridge University Press: Cambridge, 1964.

(29) (a) Mabbs, F. E.; Machin, D. J. *Magnetism and Transition Metal Complexes*; Chapman and Hall: New York, 1973. (b) Goodenough, J. B. *Magnetism and the Chemical Bond*; John Wiley and Sons: New York, 1963. (c) Chikazumi, S. *Physics of Magnetism*; John Wiley: New York, 1978.

(30) Néel, L. *Ann. Phys.* **1948**, *3*, 137.

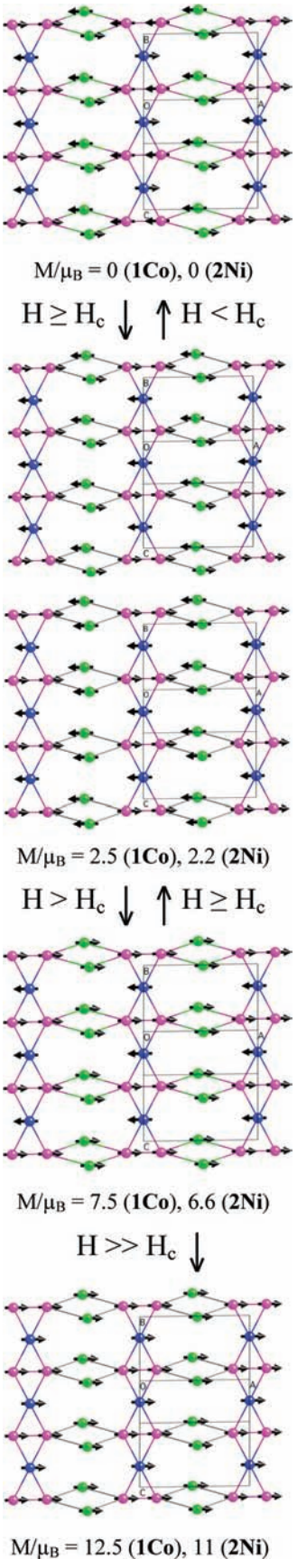

Figure 10. Proposed magnetic structures in the four states as a function of increasing magnetic field (top: $H = 0$, middle: $H \geq H_c$, bottom: $H \gg H_c$); edge-sharing M1 in purple, corner-sharing M3 in blue, and chain bridging M2 in green.

chains within each layer are antiparallel to one another; the other is where they are parallel to each other within the layer, but they are antiparallel with respect to those in adjacent layers. Likewise, the moments of the metal atom (M2) bridging the chains can be antiparallel to one another within the layer or they are parallel within a layer but antiparallel to those in adjacent layers. For the low values of the critical metamagnetic fields, the first model appears to be more plausible. Given the lack of direct bonding between the layers and the long separation between them, we anticipate the critical field for the second model to be much lower. There are several steps that can take place to bring the moments from being completely compensated, that is zero resultant moment, to being fully aligned in one direction as for a ferromagnet, where the expected saturation moments are ca. 12 μ_B for **1Co** and 11 μ_B for **2Ni**. The first anomaly in the experimental data is, therefore, the reversal of the moments of adjacent chains within a layer resulting to a ferrimagnet with the moments of the bridging cobalt atoms (M2) canceling each other or being paramagnetic. Thus, the resultant moment at this point is that of one metal center, which amounts to 2.4 μ_B for **1Co** and 2.2 for **2Ni**. Following this metamagnetic moment reversal, the magnetization is not linear, as may be expected if the moments are strongly AF coupled, but is curved to a lower saturation value than is expected for all the moments being parallel. The curved behavior indicates that there is a paramagnetic component, which may be associated to the bridging cobalt or nickel atoms. The saturation values of 7.4 and 6.7 μ_B, therefore, suggest that there is a resulting three metal moment which may be counted as follows: the moments within the chains remain the same (a ferromagnetic edge-shared pair (M1) and an antiferromagnetic corner-shared pair (M3)) and those of the bridging ones (M2) are aligned parallel with the ferromagnetic pair (M1). This conclusion is derived from the expected hierarchy of the exchange energies between the three crystallographic independent metals as given in Table 3; that is in the following order J(M1−M3) > J(M1−M1) ≫ J(M2−M1 or M3) ≫ J(interlayer). Thus, the effect of increasing the applied field is to overcome these exchange interactions in the reverse order.[29c]

Conclusion

$[M^{II}_5(OH)_2(chtc)_2(H_2O)_{10}]\cdot 2H_2O$, M = Co or Ni, are two unique systems where long-range magnetic ordering, 5.8 K (M = Co) and 3.0 K (M = Ni), is unexpectedly observed from one-dimensional magnetic chains connected by bridges of several nonmagnetic and magnetic ions. The field dependence of the magnetization provides evidence of sequential reversal of the moments, going from an antiferromagnet with fully compensated moments in zero field through a metamagnetic transition at low field of 150 Oe (M = Co) and 300 Oe (M = Ni) to a ferrimagnet with one residual moment and finally progressing gradually to a ferrimagnet with three moments. We propose consequently a magnetic ordering mechanism.

Acknowledgment. This work was funded by the CNRS and Kyushu University. We thank Nathalie Kyritsakas (Université de Strasbourg) for the single crystal structure

determination. K.O. thanks Kyushu University for a grant to visit Strasbourg University and Strasbourg University for its hospitality. M.K. is grateful to JSPS for an Invitation Fellowship Program for Research in Japan (Short Term) short-term fellowship and to JST Promoting Globalization on Basic Research Programs. S.T. is grateful to JSPS for a Grant-in-Aid fund for Scientific Research (C) (20540336).

Supporting Information Available: Two CIF files; check CIF/PLATON report; figure of numbering scheme; X-ray powder diffraction patterns of **1Co** and **2Ni**. This material is available free of charge via the Internet at http://pubs.acs.org.